Journal: Physical Review E

Accession code: EF12816

Article Title: Self-assembled clusters of mutually repelling particles in confinement

First Author: P. D. S. de Lima

AUTHOR QUERIES - TO BE ANSWERED BY THE CORRESPONDING AUTHOR

The following queries have arisen during the typesetting of your manuscript. Please answer these queries by marking the required corrections at the appropriate point in the text.

1	Table II is already cited in text. Is this additional Appendix paragraph necessary? Yes please
2	Please note that duplicate reference were detected (i.e., Refs. [52] and [54]) and provide instructions for which should be deleted or amended. We can perform renumbering of references if you provide simple instructions. no duplicate!
FQ	This funding provider could not be uniquely identified during our search of the FundRef registry (or no Contract or Grant number was detected). Please check information and amend if incomplete or incorrect.

1: Yes, please keep the Appendix paragraph for further information to the reader

2: Refs [52] and [54] are not duplicates, but different publications. Please keep them both.

FQ: requires Simon

PHYSICAL REVIEW E **00**, 004100 (2025)

Self-assembled clusters of mutually repelling particles in confinement

P. D. S. de Lima,[1,*] R. De La Cour,[2,3] K. Gaff,[2] J. M. de Araújo,[1] S. J. Cox,[4] M. S. Ferreira,[2,5] and S. Hutzler[2]

[1] *Departamento de Física Teórica e Experimental, Universidade Federal do Rio Grande do Norte, 59078-970 Natal-RN, Brazil*
[2] *School of Physics, Trinity College Dublin, Dublin 2, Ireland*
[3] *School of Physics, Technological University Dublin, Dublin 7, Ireland*
[4] *Department of Mathematics, Aberystwyth University, Aberystwyth, Ceredigion, SY23 3BZ Wales, United Kingdom*
[5] *Centre for Research on Adaptive Nanostructures and Nanodevices (CRANN) & Advanced Materials and Bioengineering Research (AMBER) Centre, Trinity College Dublin, Dublin 2, Ireland*

(Received 24 June 2025; accepted 3 September 2025; published xxxxxxxxxx)

Mutually repelling particles form spontaneously ordered clusters when forced into confinement. The clusters may adopt similar spatial arrangements even if the underlying particle interactions are contrastingly different. Here, we demonstrate with both simulations and experiments that it is possible to induce particles of very different types to self-assemble into the same ordered geometric structure by simply regulating the ratio between repulsive the ~~repulsion~~ and confining forces. This is the case for both long- and short-ranged potentials. This property is initially explored in systems with two-dimensional circular symmetry and subsequently demonstrated to be valid throughout the transition to one-dimensional structures through continuous elliptical deformations of the confining field. We argue that this feature can be utilized to manipulate the spatial structure of confined particles, thereby paving the way for the design of clusters with specific functionalities.

DOI: 10.1103/1wcz-hhw6

I. INTRODUCTION

Understanding the mechanisms that govern the formation and evolution of particle clusters is of fundamental interest in scientific areas as diverse as statistical physics [1,2], condensed matter physics [3–5], and astrophysics, to name a few. The composing particles may be magnetic [5–8] and/or ionic [9], thermally and/or optically active [10], and may range in size from nanometers up to very large scales [11,12]. The breadth of particle types and sizes of these clusters means that they may be controlled through different types of force fields, suggesting diverse applications [13–16]. The coexistence of two competing force fields acting on the particles is what drives their spontaneous clustering: one that traps them within a restricted area of space and a pairwise repulsion that prevents them from coalescing into a high-density region.

Authors of previous studies of such clusters (sometimes referred to as *classical Wigner clusters* [17]) have reported that particles may self-assemble into similar spatial arrangements when their underlying interactions are not too different. Numerical results were obtained for particles placed in a harmonic (circular) confining potential and interacting via a Coulomb potential [18–20] but also for elliptic confinement, with particles interacting via Coulomb [21] or a Yukawa potential [22,23], or with a logarithmic force law [24]. In Ref. [23], a parameter could be varied to approximate arrangements of hard spheres in confinement; Ref. [25] is an online circle database of conjectured optimal ~~sphere~~ packings in circular confinement, obtained computationally, for a large range of circle ~~sphere~~ numbers. Experimental studies include arrangements of magnetic particles [8,26–29] or those interacting via a Coulomb potential [30,31].

In this article, we argue that the conditions that interaction potentials must obey to generate clusters with the same equilibrium structure might be much less restrictive than previously thought. As a result, it is possible to identify systems that, at first glance, have very little in common with one another and yet display similar geometrical layouts. In fact, here, we bring together examples of electrically charged particles, magnetic dipoles, hard spheres, and bubbles in a liquid foam, all under a common framework. We show that a simple model based on the repulsion-confinement ratio can describe cluster formation in widely diverse systems. This suggests a strong degree of universality of self-assembled particle clusters in general, as seen in Table I, where three of the aforementioned systems display similar geometrical arrangements, even though the nature and the range of the interaction between the parts are totally different.

In unconfined two-dimensional (2D) systems, the equilibrium state of repelling particles, for most forms of interaction, is the familiar triangular lattice [33]. What is evident from the photographs in Table I is that confinement and small system size break this translational invariance, resulting in the types of intricate arrangements that are discussed within the framework of general packing problems [34].

In the following, we focus on the evolution as particles initially confined to a 2D environment are ~~deformed~~ toward forced a one-dimensional structure. For simplicity, we constrain the clusters to elliptical geometries, where a circle (of eccentricity $\epsilon = 0$) can be continuously transformed into a line as $\epsilon \to 1$.

Published results regarding particles in elliptical confinement appear to be limited, motivating our experiments, depicted in Table I, and the simulations that follow. Saint

*Contact author: paulo.douglas.lima@fisica.ufrn.br

TABLE I. Interacting particles in confinement arrange themselves in similar configurations, despite the very different physical nature of their interactions. The table shows photographs of $N = 5$ and 10 close-packed hard spheres, magnetically active particles in the form of floating dipoles, and soap bubbles. All are confined within ellipses, for five different values of eccentricity $\epsilon = 0, 0.44, 0.66, 0.87$, and 0.95. (Details about the respective experimental setups are provided in Sec. III.) Alternative arrangements exist (see Table II); here, we show only those of minimal energy, as identified in computer simulations (Sec. IV). The hard-sphere packings for $\epsilon = 0$ (circular confinement) correspond to conjectured densest circle packings, as obtained from simulations [25], also $N = 5$, $\epsilon = 0.87$, and $N = 10$, $\epsilon = 0.66$ [32].

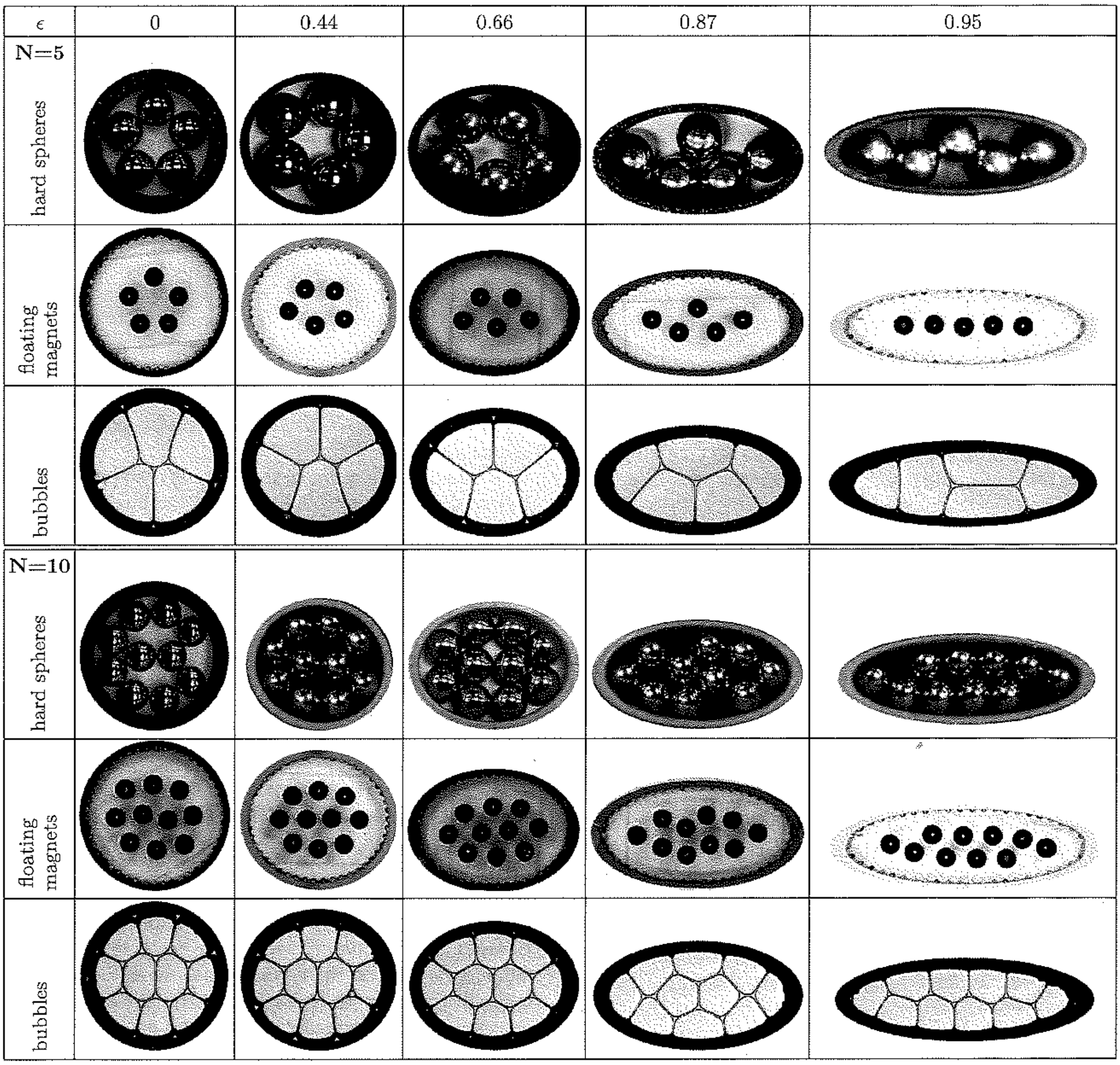

Jean and Guthmann [31] performed experiments with electrically charged stainless steel balls placed within a charged elliptic confinement. The structures they found are consistent with our results, as will be discussed in Sec. VI. Systematic computational results for particles confined within an ellipse also appear to be limited, due to the much more demanding computation in determining circle-ellipse overlaps. For the hard-sphere problem, Birgin *et al.* [35] described a nonlinear optimization procedure which computes dense packings of disks within an ellipse. (Their main interest, however, relates to algorithm efficiency.) Amore *et al.* [36] computed the variation in packing density with the shape of the ellipse for a limited range of numbers of particles. eccentricity

The structure of the manuscript is as follows. The next section introduces the model that will guide us throughout the manuscript to describe the equilibrium configurations of the particles in all the clusters. In addition, we demonstrate that, under certain conditions, it is possible for a cluster to retain its equilibrium configuration even if the interaction between the composing particles is drastically modified. Sections III and IV present a summary of experimental and numerical results, respectively, obtained for a number of different systems. The particle arrangements themselves are discussed in Sec. V. Finally, Sec. VI addresses the potential impact of our findings and how they can be used in real applications.

II. GUIDING MODEL

To illustrate our theoretical argument, we start by considering a confining region of size R and finding the exact equilibrium configuration of a cluster composed of particles interacting through the pairwise central potential energy

$$u(r) = u_0\left(\frac{r}{R}\right)^{-\alpha}, \tag{1}$$

where r is the distance between particles, and α is a dimensionless exponent. The constant u_0 has dimensions of energy, its value ~~but its exact form~~ depends on the nature of the interaction. For example, it is proportional to the product of charges in the case of Coulomb interaction and to the product of magnetic moments in the case of interacting magnetic dipoles. The exponent α defines not only the type of particle interaction described by Eq. (1) but also gives an indication of its effective range. It is instructive to separate the different confining symmetries between circular and elliptic since the former provides a much simpler illustrative picture.

A. Circular confinement

For particles contained within a circular confinement of radius R, we introduce the dimensionless distance ρ as $\rho = r/R$. We can then rewrite Eq. (1) in the dimensionless form

$$U(\rho) = \frac{u(r)}{u_0} = \rho^{-\alpha}. \tag{2}$$

For simplicity, it is convenient to have the Coulomb interaction as a reference, i.e., $\alpha = 1$. Let us then consider a cluster composed of N charged particles in the presence of a circularly confining force field. We choose the latter to be generated by M charged particles whose charges are smaller than those of the cluster by a factor λ, where λ is a dimensionless positive constant. It is worth recalling that the cluster formation results from a competition between confinement and repulsion, and the parameter λ plays a key role in regulating the balance between the two.

These M particles are uniformly distributed around the perimeter of a circle of radius R and fixed, whereas the N cluster-composing particles are allowed to move toward their respective equilibrium positions. Figure 1(a) displays a schematic representation of this cluster with $N = 5$ (white dots) and $M = 36$ (not shown). Thanks to the circular symmetry combined with the central nature of the interactions, the cluster particles lie on a ring of radius ρ around the center. The value of λ determines the radius ρ, which gets larger (smaller) as λ increases (decreases). For the case illustrated in Fig. 1(a), finding ρ consists of carrying out an energy balance between the repulsive and the confining contributions to the total potential energy. More specifically, the total potential energy of a particle is

$$U_{\text{tot}}(\rho) = U_C(\rho) + \lambda U_R(\rho), \tag{3}$$

where

$$U_R(\rho) = \frac{1}{2^{\alpha/2}\rho^{\alpha}} \sum_{j\neq 1}^{N} \left[1 - \cos\left(\frac{2\pi j}{N}\right)\right]^{-\alpha/2}, \tag{4}$$

and

$$U_C(\rho) = \sum_{k=1}^{M} \left[1 + \rho^2 - 2\rho\cos\left(\frac{2\pi k}{M}\right)\right]^{-\alpha/2}. \tag{5}$$

Equation (4) corresponds to the repulsion felt by one particle due to all the others in the cluster, whereas Eq. (5) comes from the confining forces exerted by the M particles on the boundary. The indices j and k refer to the cluster and boundary particles, respectively. Being in equilibrium means that $\partial U_C/\partial\rho = -\lambda\partial U_R/\partial\rho$.

It is worth mentioning that, at this point, no restrictions are being made on whether this equilibrium configuration falls into a local or a global minimum of the total potential energy U_{tot}. Furthermore, despite using $\alpha = 1$ for generating Fig. 1(a), the experimental results appearing on the leftmost column of Table I are all very similar, even though none of them are mediated by the Coulomb interaction.

Regarding the generic forms of U_R and U_C written in terms of α, we impose no constraint on this exponent other than it having to be positive. It is then straightforward to see that the derivative of the repulsive term diverges in the limit that $\rho \to 0$, decaying monotonically to a finite value when $\rho \to 1$. On the other hand, the derivative of the confining term vanishes at $\rho = 0$ and increases as $\rho \to 1$. Therefore, there will always be a value of $0 \leqslant \rho \leqslant 1$ for which $\partial U_{\text{tot}}/\partial\rho = 0$. This is illustrated in Fig. 1(b), which plots $-\lambda\partial U_R/\partial\rho$ (solid blue line) and $\partial U_C/\partial\rho$ (solid orange line) for the Coulomb case. Assuming $\lambda = 1$ in this instance, both curves cross at $\rho = 0.49$. A vertical dotted line indicates where the crossing occurs.

Let us now consider $\alpha \neq 1$. Since the repulsive contribution is modulated linearly by the parameter λ, it is always possible to find a suitable value for that quantity to keep the equilibrium position unchanged. In fact, the dashed lines of Fig. 1(b) correspond to $\alpha = 3$, where $\lambda = 2.2$ has been adjusted to maintain the solution at $\rho = 0.49$, i.e., such that both curves cross right where the vertical dotted line is placed. The inset of Fig. 1(b) displays the relationship between λ and α required to sustain the equilibrium position unchanged for three separate values of ρ, namely, $\rho = 0.2$ (solid line), $\rho = 0.5$ (dashed line), and $\rho = 0.8$ (dot-dashed line). To summarize, we argue that a model with an adjustable repulsion-confinement ratio λ can be employed to describe the exact equilibrium configuration of particle clusters in circular confinement, regardless of the underlying interaction. Strictly speaking, this argument works for a single shell but is sufficient to indicate the similarities in topology between different clusters.

The competition between repulsive and confining interactions is crucial for explaining particle cluster formation. As shown in Fig. 1, the repulsive potential must decay from the cluster center, while the confining potential must increase radially, both monotonically. This raises the question of what

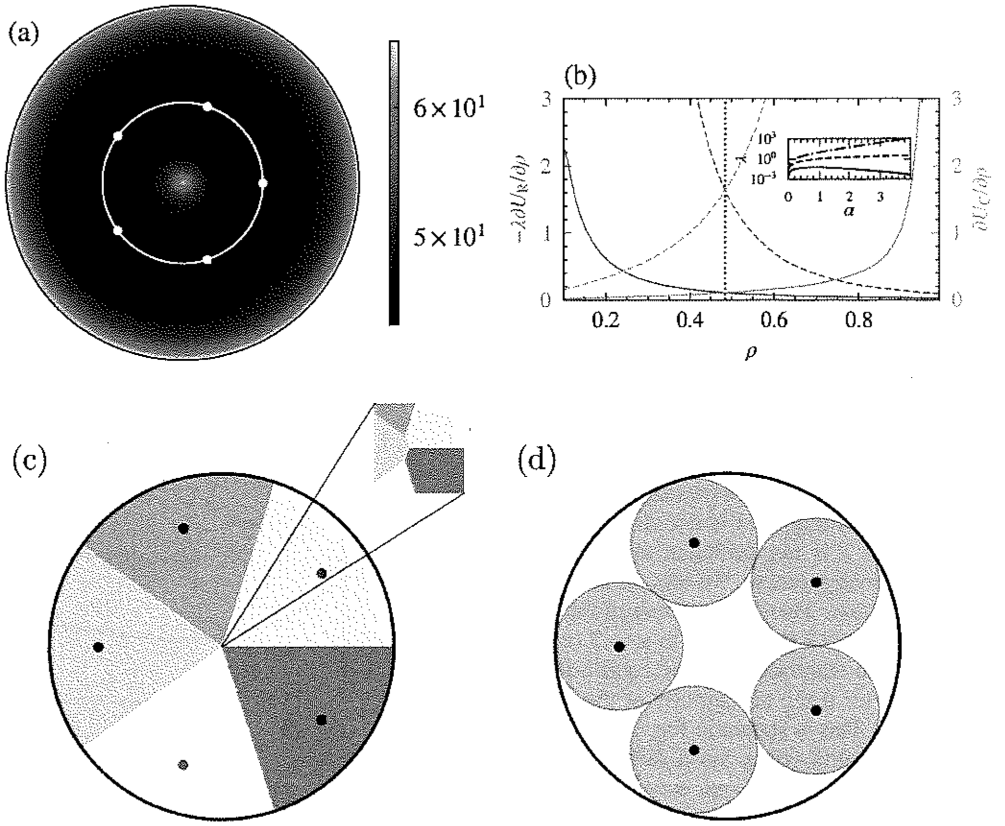

FIG. 1. (a) Colour plot indicating the total potential energy $U_{\rm tot}$ given by Eq. (3) for $N = 5$ particles (seen as white dots) around a circular ring of radius ρ and by a total of $M = 36$ particles (not shown) homogeneously distributed at the circular boundary of unit radius. The value of $\lambda = 1$ was chosen arbitrarily, and $U_{\rm R}$ and $U_{\rm C}$ are defined by Eqs. (4) and (5) with $\alpha = 1$. The white ring on which the N particles are located indicates the equipotential. The color code is such that bright (dark) colors indicate relatively high (low) potential values. (b) Radial plots (in arbitrary units) of the derivatives $-\lambda\, \partial U_{\rm R}/\partial\rho$, shown in blue (on the left axis), and $\partial U_{\rm C}/\partial\rho$, shown in orange (on the right axis). The solid (dashed) lines are for $\alpha = 1$ and $\lambda = 1$ ($\alpha = 3$ and $\lambda = 2.2$). The vertical dotted line indicates that the solid lines cross at the same value of $\rho = 0.49$ as the dashed lines. The inset displays the relationship between λ and α required to have the $N = 5$ particles at equilibrium at values $\rho = 0.2$ (solid line), $\rho = 0.5$ (dashed line), and $\rho = 0.8$ (dot-dashed line). (c) Voronoi structure obtained through a simple energy minimization of the guiding model with $N = 5$ and λ selected through the criterion of minimizing the variance in the areas of the Voronoi cells. The central part, enlarged in the inset, is topologically equivalent to the corresponding soap bubble experiments in Table I. (d) Hard-sphere equilibrium configuration obtained through the same energy minimization procedure but this time by adjusting λ to maximize the volume fraction of the cluster.

happens when interactions become short-ranged (e.g., contact forces) instead of following a power law. Two examples in Table I, hard spheres and soap bubbles in confinement, demonstrate short-ranged interactions. For these, the absence of forces when objects are not in contact requires a modified strategy to determine the appropriate value for the parameter λ, different from the method in Fig. 1(b). We will discuss this next.

For the hard spheres, for example, it is possible to find close-packing solutions by following a simple procedure. We minimize the total energy defined in Eq. (3), with any value of α, say $\alpha = 1$. We then proceed to find the value of λ by imposing as an additional criterion that the packing fraction (area of $N = 5$ circles divided by confinement area) must be maximum. Figure 1(d) shows the solutions obtained for the case of $N = 5$. This corresponds to the packing fraction $\phi = 0.6845$, which coincides with the exact value reported in Ref. [25].

A similar procedure is employed for the case of bubbles, the main difference being the criterion imposed to specify the parameter λ. It is convenient to draw the particles as points (obtained through energy minimization with an arbitrary exponent α) together with the Voronoi diagram, that is, a representation in which the space is divided into polygonal-shaped regions that are closest to each of the particles. In addition to being a valuable visual aid, the Voronoi cells reflect the number of nearest neighbors a given particle has (through the number of edges) as well as the particle density (through the reciprocal of the polygonal area).

Our bubble experiments (Table I and Sec. III) were conducted with monodisperse bubbles. In our model, we can impose equal Voronoi cell areas $A_i^{\rm vor}$ by finding a value of λ which minimizes the area dispersion $\sigma^2 = (1/N)\sum_{i=1}^{N}(A_i^{\rm vor} - \langle A^{\rm vor}\rangle)^2$. This is shown in Fig. 1(c) for the case $N = 5$. It is important to stress that this simplified use of the guiding model serves in no way as a replacement to the standard way of describing the geometry of liquid foams, described in Sec. IV A. The picture described here in terms of polygonal cells disregards the pressure differences between neighboring bubbles, which lead to cell walls being arcs of circles and yet, remarkably, is capable of obtaining the same topologies, by which we mean the number of neighbors of each region, as the results depicted in Table I. The inset in Fig. 1(c) shows that what at first glance may seem like a distinct topology in this highly symmetrical particle arrangement is identical to the one seen in Table I. Therefore, it is yet another piece of evidence supporting our claim that seemingly disparate physical systems may display very similar arrangements.

B. Elliptic confinement

A similar argument to the one just presented applies when the symmetry of the confining field is not circular but elliptic. A single parameter λ is not sufficient to determine the required equilibrium configuration. We use, in addition, the eccentricity ϵ of the ellipse. Then if the nature of the interaction changes, say from $\alpha = 1$ (Coulomb) to $\alpha = 3$ (magnetic dipolar), it is possible to maintain the same equilibrium configuration of the particles if the eccentricity of the confining ellipse is also changed. This is shown in Fig. 2(a), where two sets of $N = 5$ particles interacting via a different potential are confined within ellipses of different eccentricities. When superposed, the equilibrium positions of the two sets are the same, bar small numerical deviations. In other words, like the circular case seen in Fig. 1, it is possible to identify the same equilibrium configurations of particle clusters that are governed by distinct interactions. In the same spirit, the thick solid line in Fig. 2(b) indicates what eccentricity values ϵ one would need to produce the same equilibrium configuration as in panel (a) for values of α other than 1 and 3. In addition, three other curves are shown reflecting the precise equilibrium configurations found for the floating magnets in Table I. Finally, the four configurations seen in panel (b) will remain the same if the parameter λ changes with α, as shown in panel (c). This feature once again highlights a high degree of universality in the formation of self-assembled clusters, suggesting that these similarities are likely to occur even beyond the circular and elliptical confinements considered here.

In summary, the guiding model encapsulates mutually repelling particles under the action of confining forces. Once the confinement-repulsion ratio is adjusted together with the eccentricity, it is possible to find the same equilibrium configurations regardless of the underlying interaction potentials. In the next section, we describe how we were able to experimentally generate similar equilibrium structures in clusters governed by very different physical interactions (using hard spheres, magnetic particles, and bubbles; for Coulomb interactions see Refs. [30,31]), all of which under the action of circular and elliptical confining fields.

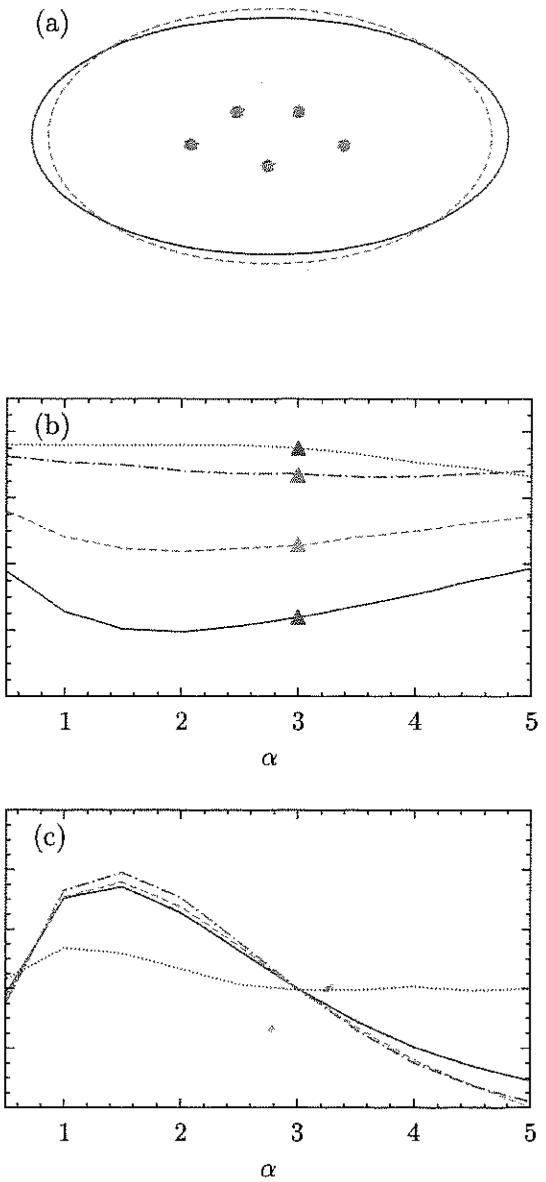

FIG. 2. (a) Example of identical equilibrium configuration for $N = 5$ particles under different interaction potentials. The orange stars correspond to the Coulomb case ($\alpha = 1, \lambda = 1.3, \epsilon = 0.91$) and the blue circles to the magnetic case ($\alpha = 3, \lambda = 1, \epsilon = 0.87$), both with $M = 36$ and ellipses in the same color. (b) This plot indicates the relationship between the eccentricity of the confining ellipse and the exponent α required to maintain a given equilibrium configuration. The four points highlighted at $\alpha = 3$ are the elliptical eccentricity values seen in Table I, namely, $\epsilon = 0.44$ (blue triangle), 0.66 (orange triangle), 0.87 (green triangle), and 0.95 (red triangle), for the case of $N = 5$ floating magnets. (c) This plot indicates how the parameter λ must change with α to maintain the same four equilibrium configurations highlighted in panel (b).

III. EXPERIMENTAL REALISATIONS OF PACKINGS IN ELLIPSOIDAL CONFINEMENT

In both the experiments described in this section and the simulations of Sec. IV, we restrict ourselves to elliptical confinements of five different values of eccentricity, $\epsilon \in \{0, 0.44, 0.66, 0.87, 0.95\}$, where $\epsilon = \sqrt{1-(b/a)^2}$, with a and b denoting, respectively, the lengths of the semimajor and semiminor ellipse axes. Experimental results are described for $N = 5$ and 10 particles.

A. Experiments with hard spheres

Experimenting with dense packings of hard spheres is probably the simplest way to illustrate the role that confinement plays in the formation of ordered arrangements. The structures encountered for given values of eccentricity ϵ and number of spheres N will also be identified in our experiments with floating magnets and bubbles.

Since we are only considering a monolayer of spheres, the packings are equivalent to the problem of the densest 2D packings of nonoverlapping hard disks in confinement. In this context, the problem may be stated as follows. Given an ellipse of area A and eccentricity ϵ, what is the area A_c, of identical circles that maximize the packing fraction $\phi = NA_c/A$, for a given number N of circles?

For the case of a *circular* confinement, i.e., $\epsilon = 0$, there is an online database [25] of conjectured optimal packings, obtained computationally, for values of N up to 2604. However, systematic computational results for confining ellipses appear to be limited, due to the much more demanding computation in determining circle-ellipse overlaps. Birgin *et al.* [35] described a nonlinear optimization procedure which computes over dense packings of ~~∼~~300 circles within an ellipse. However, their main interest relates to algorithm efficiency. Amore *et al.* [36] computed the variation in packing density with the length of the semimajor axis for three values of N (37, 61, 91); some further simulation results are displayed in Ref. [32].

Here, we describe an illustrative experimental approach to obtain dense sphere packings in confinement. It involves the use of sets of metal spheres (with a different sphere diameter in each set) and three-dimensionally (3D) printed elliptical frames of different areas for the five different values of eccentricity, as stated above. We validate our results by comparing with conjectured optimizers for $N = 5, \epsilon = 0.867$ and $N = 10, \epsilon = 0.6539$ [32].

To obtain a dense sphere packing for a given elliptical frame, we proceed as follows. The frame is placed on a horizontal surface, and we manually dispose spheres of a given size into it. This process generally does not result in a dense packing, i.e., there comes a point when there is enough room available for the spheres to rattle but not enough room for the addition of a further sphere, without losing contact with the horizontal surface. We thus start the process again but now with slightly larger or smaller spheres. By trial and error, we minimize the amount of free space to arrive at a (near) dense configuration.

Table I shows photographs of the arrangements that we consider sufficiently space-filling to demonstrate a dense packing. For the circular confinement, $\epsilon = 0$ (for which we have simulated data to compare with [25]), we reproduce the conjectured densest arrangements for both $N = 5$ and 10. Our experimentally obtained values for the packing fractions are $\phi_5 = 0.68 \pm 0.01$ and $\phi_{10} = 0.69 \pm 0.01$; this is consistent with the published results $\phi_5 = 5/[1 + 1/\sin(\pi/5)]^2 \simeq 0.685$ and $\phi_{10} \simeq 0.688$ [25]. Also, our results for $N = 5, \epsilon = 0.87, \phi = 0.68 \pm 0.01$ and $N = 10, \epsilon = 0.66, \phi = 0.77 \pm 0.01$ are consistent with those of simulations ($\phi_5 = 0.6869, \phi_{10} = 0.7797$) [32].

B. Experiments with floating magnets

Experiments with mutually repelling magnets floating on water and subject to an external magnetic confining field are generally traced back to the 19th century physicist Mayer [26,27]. His main interest, and that of many others who followed, e.g., Refs. [8,28,29,37], was the identification of equilibrium structures for a *circularly* symmetric confining field. Here, we report experiments in which the confining field has elliptical symmetry, with the same values of eccentricity as given above.

Our experiments were performed using floaters made from 3D-printed hollow cylinders, open at the top (diameter 22.4 mm, height 25 mm), as illustrated in Fig. 3(a). A metallic rod (length 23 mm, diameter 4.5 mm) was led through a hole at the bottom, and two small neodymium disk magnets (diameter 5 mm, each of thickness 1.4 mm; purchased from supermagnete [38]) were attached to it at the bottom end. When placed into a pool of water, the magnet-fitted cylinders float, with the magnets being submerged in the water.

We also 3D-printed ~~four~~ elliptical frames, with the same cross-sectional area of π cm^2 but different eccentricities. Bar magnets (toy magnetic building sticks) were attached along the inner perimeter of each frame in opposite orientation to that of the floating magnets, thus providing a confining magnetic field. The same number of magnets, 42, was used for all of the frames; since the length of the perimeter of an ellipse increases with eccentricity ϵ, this results in a number density of magnets which decreases with ϵ. DELETE

The magnet-fitted elliptical frame rests on the bottom of a pool of water, and its rim projects above the water level. Magnetic floaters were then placed one by one into the frame and allowed to settle into equilibrium positions. After ∼1 minute, photographs of the resulting configurations were taken from above.

Results for $N = 5$ and 10 are shown in Tables I and II. In contrast with our hard-sphere packings, the floating magnets are in contact with neither each other nor the confining frame. Nevertheless, the arrangements of their centers are similar to those of the hard spheres. We will further discuss similarities and differences in Sec. V.

C. Experiments with monolayers of bubbles

Arrays of soap bubbles floating on a liquid (introduced by Bragg and Nye [39] to model crystal structure) serve as another simple quasi-2D experimental system to demonstrate the formation of structures with a now familiar topology when in confinement. Like the hard spheres of Sec. III A, bubbles experience repelling forces only when they are in contact with each other or with the confining frame.

In the following, we describe experiments performed with monolayers of equal-volume bubbles confined within 3D-printed elliptical frames of equal area but different eccentricity. The bubbles were produced by blowing air at constant pressure through a nozzle into a pool of aqueous surfactant solution; see Fig. 3(b). (We chose the commercial detergent Fairy Liquid, as it is known to produce stable foams.) The elliptical frame is placed at the surface of the liquid pool, so that the rising bubbles aggregate within it, with their vertical extension slightly exceeding the height of the frame rim. Once

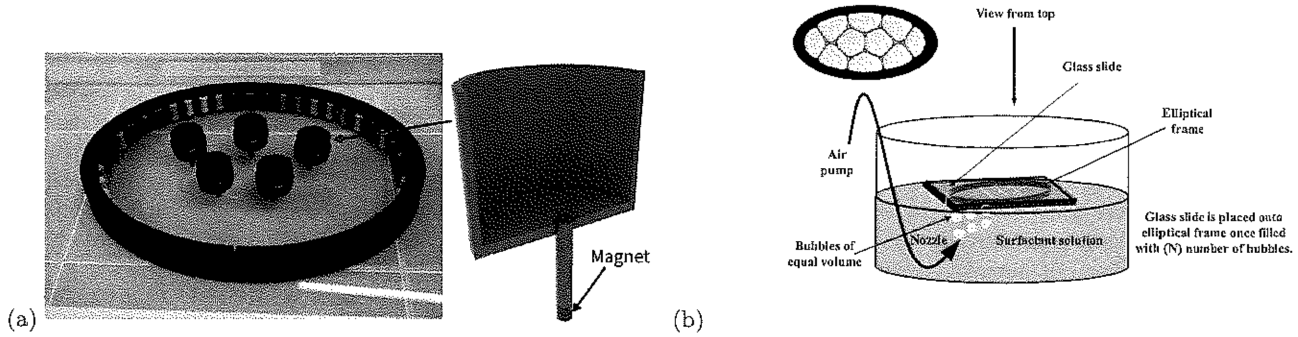

FIG. 3. Experimental setups for the creation of elliptically confined clusters of magnetic floaters or bubbles. (a) A cluster of five magnetically repelling floaters in water, confined by a ring of elliptically arranged magnets. The view of (the cross-section of) one of the floaters shows the small disk magnets that are attached at the bottom of the metal keel. (b) Monodispersity of the bubbles is ensured by having a constant air flow. Once the elliptical frame is entirely filled with bubbles, a glass cover is placed over it, contacting the bubbles. This results in a 2D cellular structure, when viewed from above.

the frame is filled with a monolayer of bubbles, a glass plate is used to cover it. Since the plate is also contacting the bubbles, this leads to a 2D confined *covered* Bragg raft, as was pioneered in the experiments in Ref. [40]). This raft is viewed from the top, resulting in an image of a 2D cellular structure.

The number of bubbles N that can be placed within an ellipse of given area depends on the size of the monodisperse bubbles. However, the quasi-2D character of the experiment, i.e., the finite vertical dimension of the raft, allows for the accommodation of a range of bubble sizes for a given value of N.

We have gathered data for $N = 5$ and 10, for a total of five different elliptical frames (eccentricity $\epsilon = 0, 0.44, 0.66, 0.87, 0.95$) and fixed frame cross-section $A = \pi$ cm^2. The equivalent sphere diameters of the bubbles in use were 3.0 mm ($N = 5$) and 2.8 mm ($N = 10$). The height of the frame rim above the water line was $\sim$2.0 mm.

For each pair of numbers of bubbles N and eccentricity ϵ, we conducted at least 10 experimental runs. This enabled the identification of several alternative bubble configurations. Table I shows the subset of structures which correspond to configurations of minimal energy, as identified in our computer simulations of 2D foams, described in Sec. IV A. Further configurations are shown in Table II.

IV. COMPUTER SIMULATIONS OF CLUSTERS IN ELLIPTICAL CONFINEMENT

A. Simulations of 2D foams

In an ideal 2D dry foam, each bubble is enclosed by soap films consisting of circular arcs that meet in threes at 120° and meet the confining walls at 90° [41,42]. We create monodisperse foam containing N bubbles in an ellipse with eccentricity ϵ using the Surface Evolver [43] in circular arc mode. The energy of a 2D foam is proportional to the total length of the soap films (the perimeter); we find local minima of the perimeter to high accuracy. We examine many local minima from which we conjecture the global minimum for each N and ϵ.

The method is based on the one described in Ref. [44]: for each N and ϵ, we find an approximation to the equilibrium position of N particles confined in an ellipse and interacting via a Coulomb interaction potential (described in more detail in Sec. IV B). These then act as seed points for a Voronoi construction, as described above. The Voronoi regions are then imported into Surface Evolver and treated as bubbles (with curved edges), and the local minimum of the total perimeter is found by gradient descent.

This is followed by a Metropolis-like shuffling procedure, in which we delete an edge, either chosen at random or the edge with the shortest length, to see if the foam perimeter is decreased—if it is, the new foam structure is kept, else it is rejected. This process results in a conjectured minimal foam for each (N, ϵ). Finally, for each of these foams, we vary ϵ over a small range (roughly ± 0.2) as a check that the foam structure of lowest perimeter has been found also at nearby eccentricities. These results are in Fig. 4.

B. Simulations of floating magnets

To predict the arrangement of floating magnets, we treat them as classical particles that interact via a pair-wise potential and are subject to a confining potential, which is a particular case of the guiding model presented in Sec. II with $\alpha = 3$. However, we stress that our method would be the same for the Coulomb case ($\alpha = 1$) [18–20,23].

In this regard, we obtain equilibrium configurations of N interacting magnetic particles possessing a magnetic moment m, which are geometrically confined in a 2D domain by M fixed magnets with magnet moment m^{ext} on the boundary of an ellipse. Assuming that all magnet moments involved are aligned with the z direction, the total energy can be written as

$$u(r) = \frac{\mu_0}{4\pi} \sum_{i=1}^{N} \sum_{k=1}^{M} \frac{m m^{\text{ext}}}{r_{ik}^3} + \frac{\mu_0}{8\pi} \sum_{\substack{j=1 \\ i \neq j}}^{N} \frac{m^2}{r_{ij}^3}, \tag{6}$$

where μ_0 is the magnetic permeability of the medium, and r_{ik} is the distance between the ith particle and kth fixed magnet,

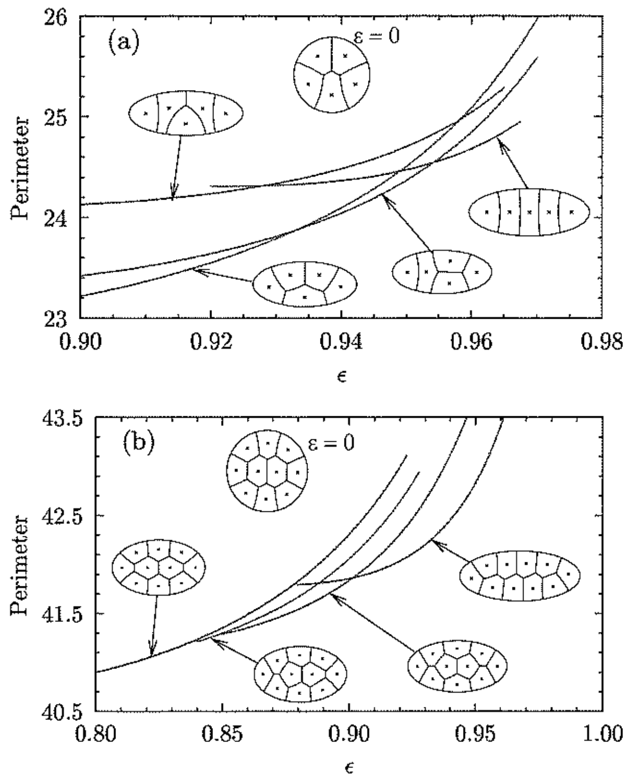

FIG. 4. Optimal arrangement of N bubbles in an ellipse with varying eccentricity ϵ. The value of the perimeter given includes the length of the elliptical frame. (a) $N = 5$. The topology of the least-perimeter cluster is the same for $0 \leqslant \epsilon < 0.93$, above which there are two further arrangements of the bubbles. (b) $N = 10$. The topology of the least-perimeter cluster is the same for $0 \leqslant \epsilon < 0.84$, above which there are several different arrangements of the bubbles, not all shown.

while r_{ij} corresponds to the distance between two moving particles. For a fixed cross-section area πab and eccentricity ϵ, as in Sec. III B, the semiaxes are given by $a = (1-\epsilon^2)^{-1/4}$ and $b = (1-\epsilon^2)^{1/4}$. This allows us to rewrite the total magnetic energy Eq. (6) in a dimensionless form

$$U_{\text{tot}} = \sum_{\substack{j=1\\ i\neq j}}^{N}[(\eta_i-\eta_j)^2+(1+\epsilon^2)(\xi_i-\xi_j)^2]^{-3/2}$$
$$+\frac{\lambda}{2}\sum_{i=1}^{N}\sum_{k=1}^{M}[(\eta_i-\eta_k)^2+(1+\epsilon^2)(\xi_i-\xi_k)^2]^{-3/2}, \quad (7)$$

where $U_{\text{tot}} = 4\pi a^3 u/(\mu_0 m m^{\text{ext}})$, with $\lambda = m^{\text{ext}}/m$. Moreover, we have defined the dimensionless coordinates $\eta_i = x_i/a$ and $\xi_i = y_i/b$, which are constraints to $\eta_i^2 + \xi_i^2 \leqslant 1$.

We use the generalized simulated annealing (GSA) method [45–48] to efficiently minimize Eq. (7) for the $2N$ equilibrium positions (η_i, ξ_i). We proceed similarly as in Ref. [8] and calibrate λ for a particular experiment, namely, $N = 5$ and $\epsilon = 0$, in which we obtain $\lambda = 1.3$. The equilibrium configurations obtained in this case are shown in Fig. 5, considering the $N = 5$ and 10 cases. Remarkably, we can reproduce the experimental observations very well regardless of the eccentricity using the same calibrated λ. It is expected since this parameter depends solely on the balance between interparticle repulsion and confinement.

V. COMPARISON OF THE DIFFERENT SYSTEMS

In Sec. III, we have presented experimental data for three different systems: hard spheres, floating magnets, and bubbles. All consist of a discrete set of interacting particles, confined by an external potential. These ingredients are sufficient to result in the same topological arrangements, despite the obvious differences in the character and nature of the respective interactions between particles. All the experimentally produced configurations are confirmed by simulations of the corresponding system, see Figs. 4 and 5.

Hard sphere interactions are discontinuous and only act upon contact; they are usually modeled using a pairwise additive Hertzian potential [49]. Bubbles also interact via contact forces. However, in contrast with hard spheres, the change in shape which they undergo upon contact results in nonlocal

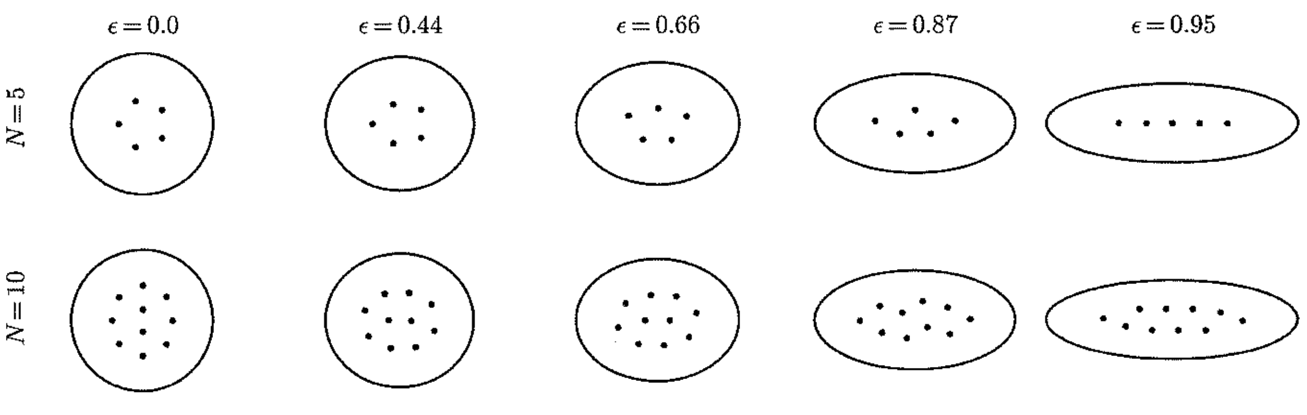

FIG. 5. The equilibrium configurations for the floating magnets simulations for $N = 5$ (top panel) and $N = 10$ (bottom panel). The parameter λ was calibrated from one experimental observation ($N = 5$, $\epsilon = 0$). The scale varies between figures with different eccentricities, but all figures share the same area.

forces, featuring a logarithmic term [50]. The floating magnets, on the other hand, are not governed by contact forces but by long-range dipole interaction.

We studied arrangements of $N = 5$ and 10 particles of the above kinds placed in an elliptic confining potential. The arrangements reveal topologically similar sequences of structures for the five different values of eccentricity ϵ that we probed. In the following, we will summarize these findings.

For $N = 5$ and $\epsilon = 0$, the centers of the particles (hard spheres/floating magnets/bubbles) can be regarded as the vertices of a (regular) pentagon (as in Fig. 1). The arrangement becomes increasingly distorted for larger values of ϵ, leading to the loss of contacts of nearest neighbors. In the limit $\epsilon \rightarrow 1$, the only possible structure is that of a straight line of particles (see Table I for floating magnets and Table II for bubbles); in the case of hard spheres or floating magnets, this straight line formed by particle centers is preceded by a zigzag arrangement (or buckled line), which straightens out with increasing ϵ.

For bubbles, the zigzag structure is replaced by an arrangement with three bubble centers situated along the major axis and two on a line perpendicular to it but not coinciding with the minor axis (see Table I, $\epsilon = 0.95$). The same arrangement can also be obtained for our floating magnets (Table II, $\epsilon = 0.87$), but in this case, it corresponds to a higher energy configuration than the zigzag structure. The arrangement was also observed by Saint Jean and Guthmann [31] in their experiments with steel spheres under the influence of Coulomb forces, for similar values of ϵ. Apolonario *et al.* [24] encountered it in their simulations of particles interacting via a repulsive logarithmic potential.

An alternative arrangement for $\epsilon = 0$ is to have one particle in the center, surrounded by four particles in contact [51] with the frame (or close to it, in the case of the floating magnets). This is shown in Table II for bubbles, floating magnets, and hard spheres. The corresponding 2D packing fraction of circles $\phi = \frac{5}{9}$ is lower than that for the case when all circles are in contact with the frame, with $\phi_5 = 0.685$ [25] (see Sec. III A). Also for 2D foams, this arrangement is not optimal; our simulations show that it is of higher energy than having all bubbles in contact with the frame. In our foam experiments, we were able to produce the higher energy structure for values of $\epsilon = 0$, 0.44, and 0.66 (see Table II). In the case of floating magnets, the configuration was only stable at $\epsilon = 0$. We associate the larger stability range found for foams with the fact that they constitute a jammed system, requiring larger forces for a possible restructuring.

For $N = 10$, a larger number of possible arrangements exists, see Tables I and II; also, here, a similarity in the sequence of the optimal structures for different values of ϵ is apparent. Let us first turn to our sphere packings, which we will again interpret as a packing of circles. The densest packing of 10 circles within a circle contains two circles in the center surrounded by eight circles in contact with the frame [25]. Each of the two central circles is in contact with three circles. Two of the perimeter circles contact three circles each, the remaining six have two contacts each. In our experiments with hard spheres, this configuration is found also for $\epsilon = 0.44$ and 0.66.

The foam structure of minimal energy resembles the hard-sphere arrangement in the following sense. It too consists of two particles (bubbles) in the center, which are surrounded by eight bubbles which contact the frame. Also, here, two types of boundary particles can be identified. There are six bubbles contacting three bubbles each and two bubbles contacting four bubbles each. Simulations show that this arrangement is that of lowest energy for $\epsilon < 0.84$; in our experiments, we found it for $\epsilon = 0$, 0.44, and 0.66.

Also, the arrangement of floating magnets (in both experiments and simulations) features two central and eight boundary magnets for $\epsilon = 0$, 0.44, and 0.66. In experiments using charged spheres, the same arrangement was reported for $\epsilon = 0.71$ [31].

At $\epsilon = 0.87$, the structure differs from that at lower ϵ in all three systems. The hard sphere structure still features two spheres that are not in contact with the frame, but each has gained an additional contact. The contact distribution of the eight boundary spheres is unchanged (6×2 and 2×3 contacts). Also, the foam still has two bubbles in the center, but each lost a side and now only contacts five boundary bubbles. Of these, there are still two types: six with four bubble contacts and two with only two contacts. The magnet configuration is probably best described as four staggered rows of two magnets, each aligned perpendicular to the major axis, and one magnet each close to the endpoints of the major axis. Two of the magnets located toward the center of the ellipse are furthest away from the frame and, in this sense, might be defined as the two nonboundary particles that are seen in both foams and hard-sphere arrangements.

At $\epsilon = 0.95$, all bubbles and all hard spheres are in contact with the frame, and there are also no more boundary magnets in the sense defined above. The configurations in the three different systems all have 180° rotational symmetry.

This type of arrangement is reminiscent of a line of hard spheres, placed in a transverse potential, which has buckled under compression [52,53]. It is tempting to pursue this analogy to explore what structural changes this would imply for this zipper structure [53] at an even higher value of ϵ, corresponding to a *weaker* compression along the major axis. As particle contacts gradually disappear (the zipper unzips), starting from the endpoints of the major axis (where there is no more room for pairs of particles), one arrives at a constellation, called the *doublet* [53], in which all particles are aligned, except one pair close to the center. A corresponding foam configuration is that for $N = 5$ at $\epsilon = 0.95$ in Table I; a corresponding magnet configuration is shown in Table II for $N = 5$ and $\epsilon = 0.87$. The suggested analogy to the buckling experiments by Refs. [52,53] also suggests the possibility of a modulated zigzag structure [54] in which the deviation of particle centers from the major-axis varies along the axis, with a maximum near the center, before at even higher values of ϵ (i.e., lower compression) a straight line is formed. We indeed found such a modulated zigzag formation in some preliminary experiments with a larger number of magnetic floaters. This could open avenues for a theoretical analysis like those in Ref. [54] in terms of a continuum model for structure formation.

VI. DISCUSSION AND OUTLOOK

Based on the guiding model of Sec. II, we have seen that mutually repelling particles in the presence of confining forces self-assemble into clusters with topologies that are primarily determined by the confinement-repulsion ratio. More specifically, in the case of circularly symmetric confinements, we have seen that it is possible to generate clusters with identical topologies even though the nature and range of the underlying interactions may be totally different. In addition, the same is possible in the case of elliptically symmetric confining forces, the main difference being that the eccentricity of the confining ellipse may be adjusted, together with the ratio of confining and repelling forces, to establish the exact cluster geometry. These findings suggest that it is possible to engineer cluster geometries whose topologies may display certain desirable functionalities [55,56]. Bearing in mind that clusters of magnetic particles are crucial in many fields, including targeted drug delivery [57], microwave absorption [58], quantum computing [59], molecular magnets and magneto-optical technologies [60–62], being able to engineer the precise topology of such structures will only widen the range of applications for these clusters.

DELETE

In the experiments that we presented, particles were placed into an elliptical frame of given eccentricity ϵ, and we recorded the resulting structure. In an alternative procedure, one could vary ϵ continuously, keeping the area of the ellipse constant, with the particles remaining confined. (This would not be possible for the hard-sphere packings, as their packing fraction varies with ϵ.) At some critical values of eccentricity, rearrangements would occur. We would also expect hysteresis, i.e., different critical values and even structures, depending on whether ϵ is increased or decreased. Experiments of this form might be difficult to devise, but simulations are possible. Indeed, the foam simulations shown in Fig. 4 were already performed by varying ϵ in small increments, for a fixed configuration. However, since we were only interested in global energy minima, we did not determine the ranges of stability for the different structures.

The results of simulating our guiding model could be presented in the form of a phase diagram, with axes of eccentricity and the parameter λ. The different phases correspond to the different structures identified, like the stability diagram for the arrangements of spheres or bubbles in a transverse confining potential [53].

In all of the above, we have only considered the (static) equilibrium configurations. The experiments using the floating magnets offer the opportunity to also study the dynamics. Some of the metastable configurations are associated with an often minute-long dance of the floaters before they settle into equilibrium. Once this is achieved, individual floaters can be manually displaced to probe the impact this shows on the other floaters. The rate of relaxation toward the old or a new equilibrium configuration indicates the steepness of the energy gradient. In our experiments with floating magnets, we observed marginally stable structures that took much longer than others to reach equilibrium. In addition, moving particular magnets can have a more significant impact on the positions of the other magnets, leading to the possibility to identify particles which have some freedom of movement and others that are locked into position. This may be related to floppy modes in condensed matter.

The extent to which similarities in the structures formed by repelling particles in confinement are found in the 3D case, with its extra degree of freedom, remains to be explored. Hard-sphere packings within spheres and Coulomb clusters in a spherical potential have been predicted up to large numbers of particles [25,63] and appear to show many similarities. However, experimental validation, even for small numbers of particles, is more difficult than in the 2D case, usually requiring advanced imaging techniques to identify the microstructure. Equilibrium states of 3D foam clusters are probably different from those of the hard-sphere case. The addition of an elliptical confinement offers an opportunity to extend the exploration of microstructural self-organization in a new direction, with new challenges for computations and experiments. In the case of floating magnets, we can imagine a vertical stack of shallow troughs that are close enough that the magnets in different layers can interact, while for foams, the challenge is in the manipulation and imaging of the resulting clusters to determine the lowest energy states.

ACKNOWLEDGMENTS

M.S.F. thanks the Federal University of Rio Grande do Norte (UFRN) in Brazil for their hospitality in early 2025, during which most of this research was conducted. This publication has emanated from research supported in part by a research grant from Science Foundation Ireland (SFI) under Grant No. SFI/12/RC2778_P2. S.H. thanks D. Weaire for continued discussions of research ideas. S.J.C. was partially supported by the Horizon 2020 Framework Programme for Research and Innovation, Grant Agreement No. 101008140 EffectFact. We also thank the anonymous reviewers for their constructive comments on the initial submission. FQ

DATA AVAILABILITY

The data that support the findings of this article are not publicly available upon publication because it is not technically feasible and/or the cost of preparing, depositing, and hosting the data would be prohibitive within the terms of this research project. The data are available from the authors upon reasonable request.

APPENDIX: FURTHER PARTICLE ARRANGEMENTS

In addition to the particle arrangements shown in Table I, a variety of alternative structures were found in our experiments, see Table II. Based on the results of our computer simulations, Sec. III, the arrangements of both floating magnets and bubbles are of higher energy. The hard-sphere circular packing has a lower packing fraction than that shown in Table I. 1

TABLE II. Some alternative arrangements obtained in experiments with 5 and 10 particle clusters in elliptical confinement, cf. Table I.

ϵ	0	0.44	0.66	0.87	0.95
N=5 hard spheres	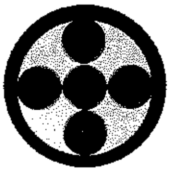 only $\epsilon = 0$ was set up for this topology				
floating magnets	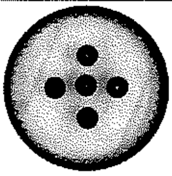 only stable for $\epsilon = 0$			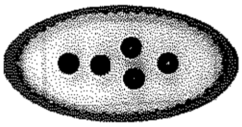	
bubbles	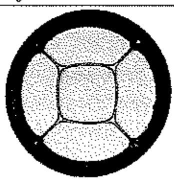	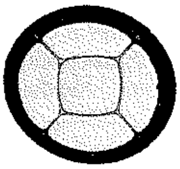	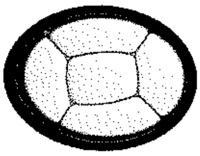		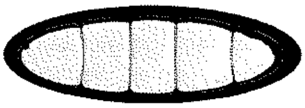
N=10 floating magnets	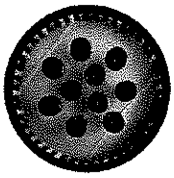 only stable for $\epsilon = 0$				
bubbles	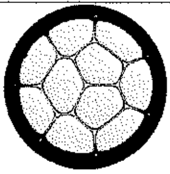	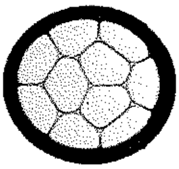	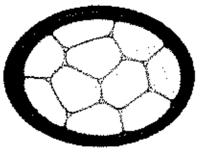 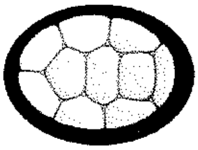	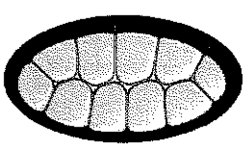 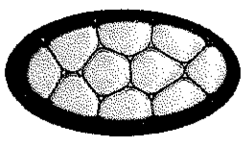	

[1] S. Agarwal, A. Dhar, M. Kulkarni, A. Kundu, S. N. Majumdar, D. Mukamel, and G. Schehr, Harmonically confined particles with long-range repulsive interactions, Phys. Rev. Lett. **123**, 100603 (2019).

[2] S. Santra, J. Kethepalli, S. Agarwal, A. Dhar, M. Kulkarni, and A. Kundu, Gap statistics for confined particles with power-law interactions, Phys. Rev. Lett. **128**, 170603 (2022).

[3] Y. Saado, M. Golosovsky, D. Davidov, and A. Frenkel, Tunable photonic band gap in self-assembled clusters of floating magnetic particles, Phys. Rev. B **66**, 195108 (2002).

[4] A. Yamilov and H. Cao, Density of resonant states and a manifestation of photonic band structure in small clusters of spherical particles, Phys. Rev. B **68**, 085111 (2003).

[5] A. A. Kuznetsov, Equilibrium magnetization of a quasispherical cluster of single-domain particles, Phys. Rev. B **98**, 144418 (2018).

[6] A. Snezhko, M. Belkin, I. S. Aranson, and W.-K. Kwok, Self-assembled magnetic surface swimmers, Phys. Rev. Lett. **102**, 118103 (2009).

[7] H. Carstensen, V. Kapaklis, and M. Wolff, Phase formation in colloidal systems with tunable interaction, Phys. Rev. E **92**, 012303 (2015).

[8] P. D. S. de Lima, A. Lyons, A. Irannezhad, J. M. de Araújo, S. Hutzler, and M. S. Ferreira, Self-assembled clusters of magnetically tilted dipoles, Phys. Rev. E **110**, 064134 (2024).

[9] H. L. Partner, R. Nigmatullin, T. Burgermeister, K. Pyka, J. Keller, A. Retzker, M. B. Plenio, and T. E. Mehlstäubler, Dynamics of topological defects in ion Coulomb crystals, New J. Phys. **15**, 103013 (2013).

[10] A. Christofi and N. Stefanou, Metal-coated magnetic nanoparticles in an optically active medium: A nonreciprocal metamaterial, Phys. Rev. B **97**, 125129 (2018).

[11] I. Theurkauff, C. Cottin-Bizonne, J. Palacci, C. Ybert, and L. Bocquet, Dynamic clustering in active colloidal suspensions with chemical signaling, Phys. Rev. Lett. **108**, 268303 (2012).

[12] L. Koehler, P. Ronceray, and M. Lenz, How do particles with complex interactions self-assemble? Phys. Rev. X **14**, 041061 (2024).

[13] M. Sarcletti, D. Vivod, T. Luchs, T. Rejek, L. Portilla, L. Müller, H. Dietrich, A. Hirsch, D. Zahn, and M. Halik, Superoleophilic magnetic iron oxide nanoparticles for effective hydrocarbon removal from water, Adv. Funct. Mater. **29**, 1805742 (2019).

[14] A. C. Gandhi, T.-Y. Li, B. V. Kumar, P. M. Reddy, J.-C. Peng, C.-M. Wu, and S. Y. Wu, Room temperature magnetic memory effect in cluster-glassy Fe-doped NiO nanoparticles, Nanomaterials **10**, 1318 (2020).

[15] D. D. Dorroh, S. Ölmez, and J.-P. Wang, Theory of quantum computation with magnetic clusters, IEEE Transactions on Quantum Engineering **1**, 5100508 (2020).

[16] Z. Liao, H. Yamahara, K. Terao, K. Ma, M. Seki, and H. Tabata, Short-term memory capacity analysis of $Lu_3Fe_4Co_{0.5}Si_{0.5}O_{12}$-based spin cluster glass towards reservoir computing, Sci. Rep. **13**, 5260 (2023).

[17] A. Radzvilavičius and E. Anisimovas, Configurational entropy of Wigner clusters, J. Phys.: Condens. Matter **23**, 075302 (2011).

[18] F. Bolton and U. Rössler, Classical model of a Wigner crystal in a quantum dot, Superlattices Microstruct. **13**, 139 (1993).

[19] V. M. Bedanov and F. M. Peeters, Ordering and phase transitions of charged particles in a classical finite two-dimensional system, Phys. Rev. B **49**, 2667 (1994).

[20] M. Kong, B. Partoens, and F. M. Peeters, Transition between ground state and metastable states in classical two-dimensional atoms, Phys. Rev. E **65**, 046602 (2002).

[21] O. Rancova, E. Anisimovas, and T. Varanavičius, Numerical modeling of structural transitions in few-particle confined 2D systems, Comput. Phys. Commun. **182**, 1914 (2011).

[22] L. Cândido, J.-P. Rino, N. Studart, and F. M. Peeters, The structure and spectrum of the anisotropically confined two-dimensional Yukawa system, J. Phys.: Condens. Matter **10**, 11627 (1998).

[23] Y.-J. Lai and L. I, Packings and defects of strongly coupled two-dimensional coulomb clusters: Numerical simulation, Phys. Rev. E **60**, 4743 (1999).

[24] S. W. S. Apolinario, B. Partoens, and F. M. Peeters, Structure and spectrum of anisotropically confined two-dimensional clusters with logarithmic interaction, Phys. Rev. E **72**, 046122 (2005).

[25] E. Specht, The best known packings of equal circles in a circle, http://www.packomania.com/.

[26] A. M. Mayer, A note on experiments with floating magnets, showing the motions and arrangements in a plane of freely moving bodies, acted on by forces of attraction and repulsion; and serving in the study of the directions and motions of the lines of magnetic force, Am. J. Sci. **s3-15**, 276 (1878).

[27] A. M. Mayer, On the morphological laws of the configurations formed by magnets floating vertically and subjected to the attraction of a superposed magnet; with notes on some of the phenomena in molecular structure which these experiments may serve to explain and illustrate, Am. J. Sci. **s3-16**, 247 (1878).

[28] H. G. Riveros, E. Cabrera, and J. Fujioka, Floating magnets as two-dimensional atomic models, Phys. Teacher **42**, 242 (2004).

[29] I. V. Nemoianu, C. G. Dragomirescu, V. Manescu, M.-I. Dascalu, G. Paltanea, and R. M. Ciuceanu, Self-organizing equilibrium patterns of multiple permanent magnets floating freely under the action of a central attractive magnetic force, Symmetry **14**, 795 (2022).

[30] M. Saint Jean, C. Even, and C. Guthmann, Macroscopic 2D Wigner islands, Europhys. Lett. **55**, 45 (2001).

[31] M. Saint Jean and C. Guthmann, Macroscopic two-dimensional Wigner asymmetric islands, J. Phys.: Condens. Matter **14**, 13653 (2002).

[32] https://erich-friedman.Github.Io/packing/cirinel/.

[33] D. Weaire and T. Aste, *The Pursuit of Perfect Packing*, 2nd ed. (CRC Press, Boca Raton, 2008).

[34] *Packing Problems in Soft Matter Physics: Fundamentals and Applications*, edited by H.-K. Chan, S. Hutzler, A. Mughal, C. S. O'Hern, Y. Wang, and D. Weaire (Royal Society of Chemistry, London, 2025).

[35] E. G. Birgin, L. H. Bustamante, H. F. Callisaya, and J. M. Martínez, Packing circles within ellipses, Int. Trans. Operational Res. **20**, 365 (2013).

[36] P. Amore, D. de la Cruz, V. Hernandez, I. Rincon, and U. Zarate, Circle packing in arbitrary domains, Phys. Fluids **35**, 127112 (2023).

[37] L. Derr, A photographic study of Mayer's floating magnets, in Proceedings of the American Academy of Arts and Sciences (JSTOR, 1909), Vol. 44, pp. 525–528.

[38] https://www.supermagnete.de/.

[39] W. L. Bragg and J. F. Nye, A dynamical model of a crystal structure, Proc. R. Soc. London A **190**, 474 (1947).

[40] M. F. Vaz and M. Fortes, Experiments on defect spreading in hexagonal foams, J. Phys.: Condens. Matter **9**, 8921 (1997).

[41] D. Weaire and S. Hutzler, *The Physics of Foams* (Clarendon Press, Oxford, 1999).

[42] I. Cantat, S. Cohen-Addad, F. Elias, F. Graner, R. Höhler, O. Pitois, F. Rouyer, and A. Saint-Jalmes, *Foams—Structure and Dynamics* (Oxford University Press, Oxford, 2013).

[43] K. Brakke, The surface evolver, Exp. Math. **1**, 141 (1992).

LEEP

[44] S. Cox and E. Flikkema, The minimal perimeter for N confined deformable bubbles of equal area, Electron. J. Combin. **17**, R45 (2010).

[45] C. Tsallis and D. A. Stariolo, Generalized simulated annealing, Physica A **233**, 395 (1996).

[46] I. Andricioaei and J. E. Straub, Generalized simulated annealing algorithms using Tsallis statistics: Application to conformational optimization of a tetrapeptide, Phys. Rev. E **53**, R3055 (1996).

[47] Y. Xiang and X. G. Gong, Efficiency of generalized simulated annealing, Phys. Rev. E **62**, 4473 (2000).

[48] Y. Xiang, S. Gubian, B. Suomela, and J. Hoeng, Generalized simulated annealing for global optimization: The GENSA package, The R Journal **5**, 13 (2013).

[49] J. Duran, *Sands, Powders, and Grains: An Introduction to the Physics of Granular Materials* (Springer-Verlag, New York, 2000).

[50] R. Höhler and D. Weaire, Can liquid foams and emulsions be modeled as packings of soft elastic particles? Adv. Colloid Interface Sci. **263**, 19 (2019).

[51] We infer contacts between spheres from the images rather than detecting them directly.

LEEP

2

[52] S. Hutzler, J. Ryan-Purcell, A. Mughal, and D. Weaire, A continuum description of the buckling of a line of spheres in a transverse harmonic confining potential, R. Soc. Open Sci. **10**, 230293 (2023).

[53] J. Ryan-Purcell, A. Irannezhad, M. T. P. Whelan, D. Weaire, A. Mughal, and S. Hutzler, Compression of a line of spheres or bubbles in a transverse confining potential, Philos. Mag. **105**, 684 (2025).

[54] D. Weaire, A. Mughal, J. Ryan-Purcell, and S. Hutzler, Description of the buckling of a chain of hard spheres in terms of Jacobi functions, Physica D **433**, 133177 (2022).

[55] P. J. Hobson, C. Morley, A. Davis, T. Smith, and M. Fromhold, Target-field design of surface permanent magnets, Phys. Rev. Appl. **22**, 034015 (2024).

[56] I. Rehberg and P. Blümler, Analytic approach to creating homogeneous fields with finite-size magnets, Phys. Rev. Appl. **23**, 064029 (2025).

[57] E. Kianfar, Magnetic nanoparticles in targeted drug delivery: A review, J. Supercond. Novel Magn. **34**, 1709 (2021).

[58] I. Shorstkii and M. Sosnin, Microwave absorption properties of Fe_3O_4 particles coated with Al via rotating magnetic field method, Coatings **11**, 621 (2021).

[59] Z. Hu, B.-W. Dong, Z. Liu, J.-J. Liu, J. Su, C. Yu, J. Xiong, D.-E. Shi, Y. Wang, B.-W. Wang *et al.*, Endohedral metallofullerene as molecular high spin qubit: Diverse Rabi cycles in $Gd_2@C_{79}N$, J. Am. Chem. Soc. **140**, 1123 (2018).

[60] J.-B. Peng, Q.-C. Zhang, X.-J. Kong, Y.-Z. Zheng, Y.-P. Ren, L.-S. Long, R.-B. Huang, L.-S. Zheng, and Z. Zheng, High-nuclearity $3d$-$4f$ clusters as enhanced magnetic coolers and molecular magnets, J. Am. Chem. Soc. **134**, 3314 (2012).

[61] C.-H. Lee *et al.*, Ferromagnetic ordering in superatomic solids, J. Am. Chem. Soc. **136**, 16926 (2014).

[62] L. Geng and Z. Luo, Magnetic metal clusters and superatoms, J. Phys. Chem. Lett. **15**, 1856 (2024).

[63] P. Ludwig, S. Kosse, and M. Bonitz, Structure of spherical three-dimensional Coulomb crystals, Phys. Rev. E **71**, 046403 (2005).